

# Stain Style Transfer using Transitive Adversarial Networks

Shaojin Cai<sup>1,2</sup>, Yuyang Xue<sup>3</sup>, Qinquan Gao<sup>1,2,3</sup>, Min Du<sup>1,2</sup>, Gang Chen<sup>4</sup>, Hejun Zhang<sup>4</sup>, and \*Tong Tong<sup>1,2,3</sup>

<sup>1</sup> College of Physics and Information Engineering, Fuzhou University, Fuzhou, China

<sup>2</sup> Fujian Key Lab of Medical Instrumentation & Pharmaceutical Technology, Fuzhou, China

<sup>3</sup> Imperial Vision Technology, Fuzhou, China

<sup>4</sup> Department of Pathology, Fujian Provincial Cancer Hospital, The Affiliated Hospital of Fujian Medical University, Fuzhou, China  
{ttraveltong}@gmail.com

**Abstract.** Digitized pathological diagnosis has been in increasing demand recently. It is well known that color information is critical to the automatic and visual analysis of pathological slides. However, the color variations due to various factors not only have negative impact on pathologist’s diagnosis, but also will reduce the robustness of the algorithms. The factors that cause the color differences are not only in the process of making the slices, but also in the process of digitization. Different strategies have been proposed to alleviate the color variations. Most of such techniques rely on collecting color statistics to perform color matching across images and highly dependent on a reference template slide. Since the pathological slides between hospitals are usually unpaired, these methods do not yield good matching results. In this work, we propose a novel network that we refer to as Transitive Adversarial Networks (TAN) to transfer the color information among slides from different hospitals or centers. It is not necessary for an expert to pick a representative reference slide in the proposed TAN method. We compare the proposed method with the state-of-the-art methods quantitatively and qualitatively. Compared with the state-of-the-art methods, our method yields an improvement of 0.87dB in terms of PSNR, demonstrating the effectiveness of the proposed TAN method in stain style transfer.

**Keywords:** Pathological Slides, Stain Transfer, Color Transfer, Generative Adversarial Networks.

## 1 Introduction

Staining is a general process in pathology. However, the differences in raw material, staining protocols and slide scanners between labs make the appearance of the pathological stain suffer from large variability. These variations not only affect the diagnosis of the pathologists [9], but also can hamper the performance of CAD systems [6].

As an alternative, algorithms for automated standardization of digitized whole-slide images (WSI) have been published [1, 2, 4, 12, 15, 17, 19, 20]. These methods can be roughly divided into three categories. **Color-matching based methods** that try to match the color spectrums between the image and reference template image. Reinhard et al. [20] matched the color-channels between the image and reference template image in the LAB color space. However, this global color mapping fails in some local regions of image, as the same transformation is applied across the whole image while ignoring the independent distributions of color in different areas of the pathological image.

In addition, **Stain separation based methods** that do the normalized operations on each staining channel independently. Macenko et al. [16] proposed the stain vectors by transforming the RGB to the Optical Density (OD) space. Khan et al. [13] assigned every pixel to the specific stain component and estimated the stain matrix. Bejnordi et al. [3] thought that these methods did not take the spatial features of the tissue into account, which might lead to improper staining. Moreover, picking a good reference image requires expert knowledge and a bad reference may hamper the performance of these methods. The third group are **Deep-learning based approaches**. These methods take advantage of the Generative adversarial networks (GANs) to transfer stain style. BenTaieb [5] designed a stain normalization net based on GANs with a discriminative image analysis model on top. However, this stain style transfer model depends on a specific model for a specific task on top. Shaban [22] proposed a method which is known as StainGAN. StainGAN is based on an Unpaired Image-to-Image Translation using Cycle-Consistent Adversarial Networks (CycleGAN). Cycle-consistency allows the images to be mapped into different color models but preserving the same tissue structure.

In this paper, we propose Transitive Adversarial Networks (TAN). TAN is also based on an Unpaired Image-to-Image Translation using Cycle-Consistent Adversarial Networks (CycleGAN) [24]. We proposed a novel generator, which can result in more accurate color transfer than other generators. TAN not only eliminates the problem of picking the reference template image but also achieve much higher quality and much faster processing speed than StainGAN, making it easier to minish the stain variants and improving the diagnosis process of the pathologists and CAD system. We have compared our method with state-of-the-art methods quantitatively and qualitatively, which demonstrates superiority of the proposed method.

## 2 Methodology

### 2.1 The Framework

Our framework is illustrated in Fig.1. TAN is an unsupervised framework based on CycleGAN [24] in stain style transfer, which allows bidirectional transference of the H&E Stain Appearance between different scanners, i.e from Aperio (A) to Hamamatsu (H) Scanner. This framework does not require paired data from different scanners. The model consists of two generators  $G_1 : A \rightarrow H$  and  $G_2 :$

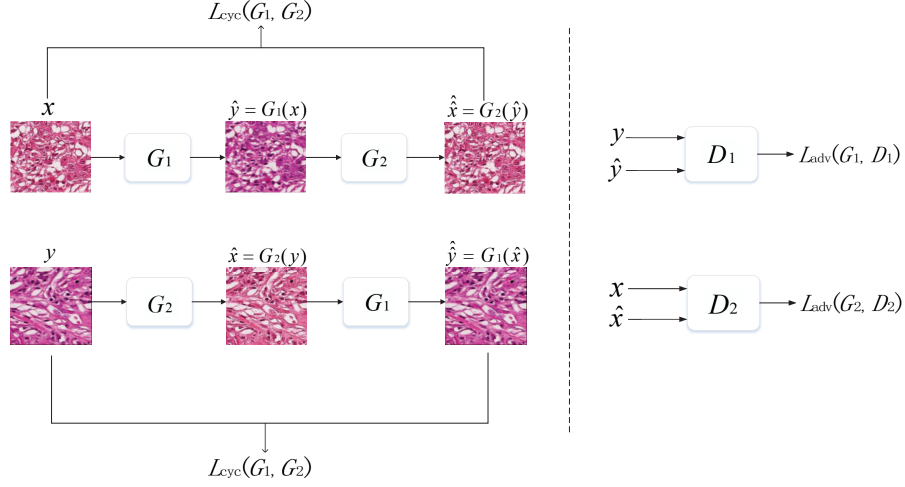


**Fig. 1.** The proposed framework for stain style transfer.  $x$  and  $y$  are unpaired images randomly sampled from their respective domains.

$H \rightarrow A$ . Each generator is trained with a corresponding discriminator,  $D_1$  and  $D_2$ . For illustration, the first pair ( $G_1$  and  $D_1$ ), try to map images from domain A to domain H. The source images  $x$  in the domain A is the input of the generator  $G_1$ , which yields generated images  $\hat{y}$ ,  $\hat{y} = G_1(x)$ . Both the generated images  $\hat{y}$  and the unpaired target images  $y$  in the domain H are treated as inputs of the discriminator network  $D_1$ . During the training process,  $G_1$  and  $D_1$  compete with each other.  $D_1$  acts as a binary classifier, trying to distinguish the generated images  $\hat{y}$  and target domain images  $y$ . Due to the adversarial training process,  $G_1$  tries to improve the quality of the generated images  $\hat{y}$  to foolish  $D_1$ . This training producer is formulated as a min-max optimization which has a adversarial loss function :

$$L_{adv}(G_1, D_1) = E_{y \sim p_{data}(y)}[\log D_1(y)] + E_{x \sim p_{data}(x)}[\log(1 - D_1(G_1(x)))] \quad (1)$$

Analogous to the first pair of the generator network  $G_1$  and the discriminator network  $D_1$ , the second pair ( $G_2$  and  $D_2$ ), try to map images from the domain H to the domain A, which replaces the input images as  $y$  and the output images as  $x$ . The training producer is also formulated as a min-max optimization process, and the loss function is  $L_{adv}(G_2, D_2)$  :

$$L_{adv}(G_2, D_2) = E_{x \sim p_{data}(x)}[\log D_2(x)] + E_{y \sim p_{data}(y)}[\log(1 - D_2(G_2(y)))] \quad (2)$$

However, if the training process is merely guided by the adversarial loss, it may result in the non-convergence of the training process and lead to model collapse. Several images from source domain will map to the single image in the

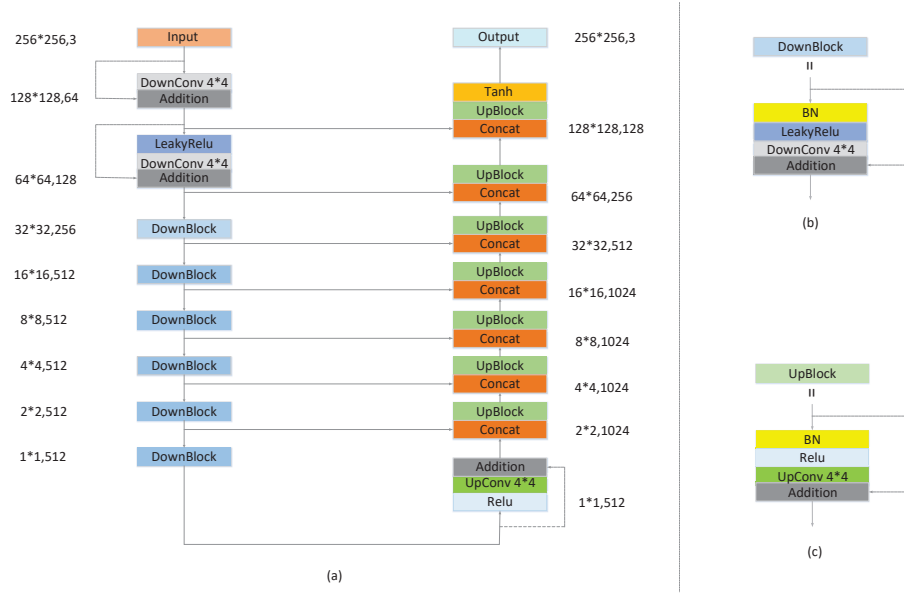


**Fig. 2.** The network of our proposed generator that we refer to as Trans-Net.

target domain if only the adversarial loss is used. Therefore, additional training constraint on the mapping function is essential. This is achieved by adding a cycle loss, which enforces the two mapping functions,  $G_1$  and  $G_2$ , to be cycle-consistent with each other. Generally speaking, two mapping functions should be reciprocal, for illustration,  $\hat{x} = G_2(G_1(x))$ ,  $\hat{y} = G_1(G_2(y))$ . This behaviour can be achieved by adding the pixel-wise cycle-consistency loss for both generators:

$$L_{cyc}(G_1, G_2) = E_{x \sim p_{data}(x)}[\|x - G_2(G_1(x))\|_1] + E_{y \sim p_{data}(y)}[\|y - G_1(G_2(y))\|_1] \quad (3)$$

As a result, the final loss for the whole training process can be described as:

$$L(G_1, G_2, D_1, D_2) = L_{adv}(G_1, D_1) + L_{adv}(G_2, D_2) + \lambda L_{cyc}(G_1, G_2) \quad (4)$$

## 2.2 Network Architectures

**Generator** Compared to U-Net, we have three innovations: i) We increase the numbers of downsampling layer and upsampling layer from 4 to 8 symmetrically, enabling the network to learn higher-level semantic information and generate more detailed context. And the experimental results demonstrate that we can produce the best images at the 8 level of downsampling. ii) As shown in Fig.2 (b) and Fig.2 (c), for each downsampling layer or upsampling layer, we add the information before sampling to the sampled information innovatively. The

operation can propagate the information from previous layer to next layer, which takes advantage of low-level features with low complexity and high-level features with high complexity, making it easier to get a smooth decision function with better generalization performance and produce more detailed results both in color and texture. iii) In U-Net, convolution operations are performed twice before each sampling operation. But in Trans-Net, we delete the two convolution operations before each sampling layer. There is no convolution layer between adjacent sampling layers, avoiding the overfitting problem. And the network only includes 16 convolution layers which is 7 layers less than U-Net, making it present a better image quality and less computation time.

The proposed generator architecture we refer to as Trans-Net is shown in Fig.2 (a). It consists of a coding operation (left side) and a decoding operation (right side). The sizes and numbers of the feature channels in every layer are written in the side of both paths. Shortcuts are used to concatenate the features from the coding phase to the decoding phase in all corresponding downsampling and upsampling blocks as shown in Fig.2 (a). This can avoid the gradient vanishing or exploding problem during backpropagation, making it easy to train deep networks.

**Discriminator** Since the  $L_1$  or  $L_2$  term can successfully capture the low-frequency information but fail to restore high-frequency information, producing blurred details on image generation tasks [14]. In order to generate both the low-frequency and the high-frequency details, we added a patch-level classifier as discriminator as proposed in [10]. This discriminator we refer to as PatchGAN can learn high-frequency features while the  $L_1$  loss can learn low-frequency features. By fusing the two types of losses, both the high-frequency and the low-frequency details can be learnt and generated. PatchGAN restricts the attention to the structure in local image patches, which penalizes the structure at the scale of  $70 \times 70$ , aiming to classify whether  $70 \times 70$  overlapping image patches are real or fake. The output of PatchGAN is a  $30 \times 30$  matrix where every element have a receptive field of  $70 \times 70$ , averaging the matrix to provide the final output.

Although patch is much smaller than the image, they can still generate high quality results with fewer parameters, and faster inference speed than that at image level. In addition, it can work on arbitrarily-sized images in a fully convolutional fashion [11]. Such a discriminator effectively models the image as a Markov random field, assuming independence between pixels separated by more than a patch diameter. The Markov random field characterize the image by local fragmentation region of pixel values. Therefore, our PatchGAN can be treated as a form of texture/style loss.

### 3 Experiments and Results

To have fair and comprehensive comparisons with other methods, we evaluated our model as follows: i) Analysis of the image quality at different levels of downsampling; ii) Analysis of the effect of the proposed generator on the results and

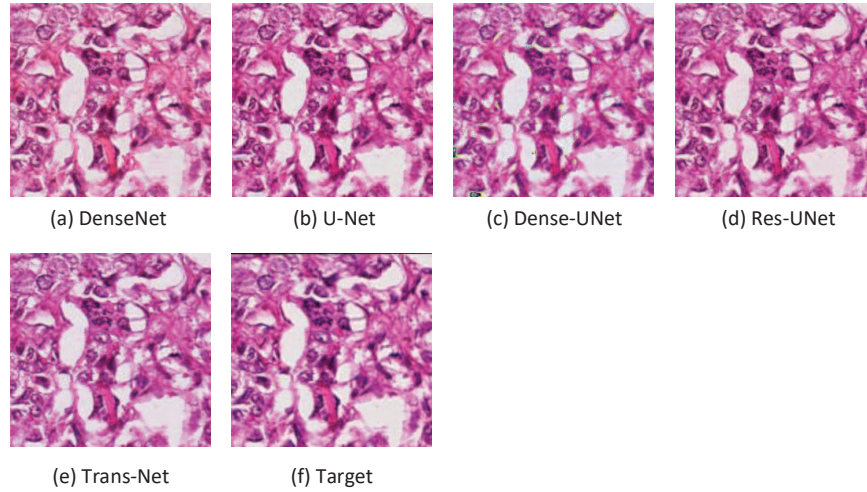


**Fig. 3.** Visual comparisons of results using different generators.

comparisons of results using different generators; iii) Quantitative and qualitative comparisons between our method and state-of-the-art approaches [22]. We will introduce the experimental dataset, the training details, the evaluational metrics and experimental results in the following sections.

### 3.1 Dateset and Details

**Dataset** The dataset is publicly available as part of the MITOS-ATYPIA14 challenge<sup>5</sup>. The dataset consists of 424 frames at  $X20$  magnification which were stained with standard Hematoxylin and Eosin (H&E). The training dataset consists of 300 frames and the test dataset consists of 124 frames. All frames were scanned by two scanners: Aperio Scanscope XT and Hamamatsu Nanozoomer 2.0-HT. Slides from both scanners were resized to identical dimensions ( $1539 \times 1376$ ). For training, we extracted 9000 unpaired patches from the training dataset of both scanners. During evaluation, we randomly extracted 620 paired patches from the testing dataset of both scanners. All patches have the same size of  $256 \times 256$ . Non-rigid registration was employed to eliminate the mismatch. Patches from Scanner H were regarded as the ground truth.

**Training details** For all experiments, we trained 9000 unpaired patches from both scanners for 6 epoches with a batch size of 1. We used the Adam solver and trained all networks with a learning rate of 0.0002. We set  $\lambda = 10$  in Equation 4.

We replaced the negative log likelihood objective for  $L_{GAN}$  by a least-squares

<sup>5</sup> <https://mitos-atypia-14.grand-challenge.org>

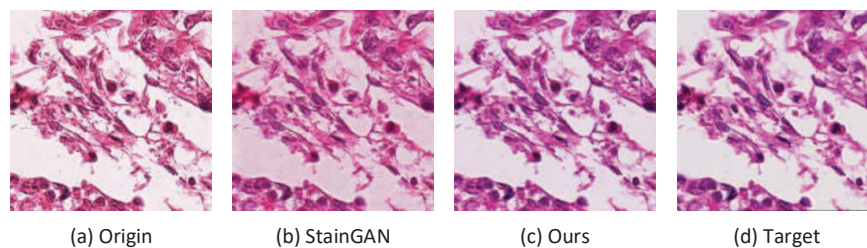


**Fig. 4.** Visual comparison between the result of our proposed method and that of StainGAN.

**Table 1.** Results of Trans-Net at different levels : Mean indicators and total processing time

Methods	PSNR	SSIM	Time (sec)
Level8	22.22	0.812	31
Level7	21.67	0.793	29
Level6	21.99	0.807	28
Level5	21.97	0.806	24
Level4	21.99	0.802	22

loss [18] and updated the discriminators using a history of generated images rather than the ones produced by the latest generators. We kept an image buffer that stores the 50 previously created images. We used this image buffer which has information of previous 50 images rather than the latest image to update the discriminators. The hardware of GeForce GTX 1080 and the PyTorch framework were used.

**Evaluation Metrics** Results were compared to the ground truth with two similarity metrics: Peak Signal-to-Noise Ration (PSNR) and Structural Similarity index (SSIM). In addition, the processing speed which is an important factor in clinical has been reported in the results. We used the total time over processing the 620 images from testing dataset to calculate the computational time.

### 3.2 Results with different levels of downsampling

It is interesting to see some results demonstrate the image quality with different levels of downsampling. We increase the numbers of downsampling layer and upsampling layer from 4 to 8 symmetrically. Results is shown in Table 1. It is obviously that the result at sampling level of 8 is the best. And the 8 level is the highest level that we can sample, because the size of our input is 256\*256 and the

**Table 2.** Comparison to other generators: Mean indicators and total processing time

Methods	PSNR	SSIM	Time (sec)
DenseNet	21.40	0.792	35
U-Net	21.95	0.802	45
Dense-UNet	20.10	0.795	119
Res-UNet	22.02	0.802	51
Trans-Net	<b>22.22</b>	<b>0.812</b>	<b>31</b>

**Table 3.** Stain Transfer Comparison: Mean indicators and total processing time

Methods	PSNR	SSIM	Time (sec)
StainGAN	21.35	0.785	60
Ours	<b>22.22</b>	<b>0.812</b>	<b>31</b>



size of the feature maps at this moment is  $1 \times 1$ . Then, we adopt 8 downsampling layers and 8 upsampling layers for our generative networks.

### 3.3 Comparisons of results using different generators

The generator of our generative adversarial networks we refer to as Trans-Net is based on the traditional U-Net structure [21]. In order to make a extensive comparisons, we replaced the generator with other network structures and compared the results using our proposed Trans-Net and other generators.

Four other network structures were used as generators for comparison, including the traditional U-Net [21] which was used in biomedical image segmentation, Res-UNet [23] which was first proposed for segmentation of retinal images, the DenseNet structure which was used in classification tasks [8], and the Dense-UNet [7] which was used to remove artifacts from the image respectively. Results are shown in Table 2. The proposed Trans-Net achieved higher values than other generators in terms of PSNR and SSIM with less computational times. The visual comparisons as shown in Fig.3, demonstrates that the results generated by the proposed Trans-Net are closer to the ground truth than the results using other generators in terms of colors, contrast and texture details.

### 3.4 Comparison with state-of-the-art method

The goal is to transfer the style of pathes from scanner A (Aperio) to the patches from scanner H (Hamamatsu) while keeping the context and texture of A. Since the medical images are unpaired in different centers, we used the cycle-consistent loss [24] to map the patches from domain A to domain H, and compared the generated patches with the real patches of scanner H (ground truth). The state-of-the-art method is StainGAN [22], the difference between TAN and StainGAN is that we have designed a novel generator we refer to as Trans-Net. The author of StainGAN adopted the architecture for their generative networks from Johnson et al. [11] who have shown impressive results for neural style transfer and super-resolution. This network contains two stride-2 convolutions, 6 residual blocks, and two stride- $\frac{1}{2}$  convolutions. Compared to the network, Trans-Net has much more stride-2 convolutions and stride- $\frac{1}{2}$  convolutions which results in more detailed semantic context information. And Trans-Net can produce much more detailed texture and color information owing to the operation that add the information before sampling to sampled information novelty. Finally, Trans-Net has only 16 convolutions, the reduction of convolutions accelerates the training speed and avoids the over-fitting problem. The results of the proposed method and StainGAN are shown in Table 3 , and Fig.4 shows their visual comparison. The PSNR value improves from 21.35 to 22.22 while SSIM improves from 0.785 to 0.812. In addition, the proposed method only requires half of the computational time of StainGAN. The visual comparison also show that the results generated by the proposed method are closer to the ground truth than the results using StainGAN.

## 4 Discussion and Conclusion

In this work, we proposed a novel method called TAN for stain style transfer. The experimental results show that the proposed method outperforms the state-of-the-art method in terms of objective metrics and visual comparisons. A new network structure called Trans-Net was proposed as generator, which contributes to better results than state-of-the-art results. There are three factors that contribute to the advantage of the Trans-Net structure: 1) It has many downsampling layers and upsampling layers to ensure the high-level semantic information can be learnt which can result in detailed texture and context. 2) It directly adds the information before and after sampling to reduce the loss of information which contributes to the much closer color and texture to the ground truth. 3) It only has 16 convolutional layers which accelerates the networks. It would be interesting to investigate how the stain style transfer affects the segmentation task and the analysis of pathological slides in our future work.

## Acknowledgement

This study was supported by the National Natural Science Foundation of China (Grant No. 6190010435) and the Science and Technology Program of Fujian Province, China (Grant No. 2019YZ016006).

## References

1. Basavanahally, A., Madabhushi, A.: Em-based segmentation-driven color standardization of digitized histopathology. In: *Medical Imaging 2013: Digital Pathology*. vol. 8676, p. 86760G. International Society for Optics and Photonics (2013)
2. Bautista, P.A., Hashimoto, N., Yagi, Y.: Color standardization in whole slide imaging using a color calibration slide. *Journal of pathology informatics* **5**, 4 (2014)
3. Bejnordi, B.E., Litjens, G., Timofeeva, N., Otte-Höller, I., Homeyer, A., Karssemeijer, N., van der Laak, J.A.: Stain specific standardization of whole-slide histopathological images. *IEEE transactions on medical imaging* **35**(2), 404–415 (2015)
4. Bejnordi, B.E., Timofeeva, N., Otte-Höller, I., Karssemeijer, N., van der Laak, J.A.: Quantitative analysis of stain variability in histology slides and an algorithm for standardization. In: *Medical Imaging 2014: Digital Pathology*. vol. 9041, p. 904108. International Society for Optics and Photonics (2014)
5. BenTaieb, A., Hamarneh, G.: Adversarial stain transfer for histopathology image analysis. *IEEE transactions on medical imaging* **37**(3), 792–802 (2017)
6. Ciompi, F., Geessink, O., Bejnordi, B.E., De Souza, G.S., Baidoshvili, A., Litjens, G., Van Ginneken, B., Nagtegaal, I., Van Der Laak, J.: The importance of stain normalization in colorectal tissue classification with convolutional networks. In: *2017 IEEE 14th International Symposium on Biomedical Imaging (ISBI 2017)*. pp. 160–163. IEEE (2017)
7. Guan, S., Khan, A., Sikdar, S., Chitnis, P.: Fully dense unet for 2d sparse photoacoustic tomography artifact removal. *IEEE journal of biomedical and health informatics* (2019)

8. Huang, G., Liu, Z., Van Der Maaten, L., Weinberger, K.Q.: Densely connected convolutional networks. In: Proceedings of the IEEE conference on computer vision and pattern recognition. pp. 4700–4708 (2017)
9. Ismail, S.M., Colclough, A.B., Dinnen, J.S., Eakins, D., Evans, D., Gradwell, E., O’Sullivan, J.P., Summerell, J.M., Newcombe, R.G.: Observer variation in histopathological diagnosis and grading of cervical intraepithelial neoplasia. *BMJ* **298**(6675), 707–710 (1989)
10. Isola, P., Zhu, J.Y., Zhou, T., Efros, A.A.: Image-to-image translation with conditional adversarial networks. In: Proceedings of the IEEE conference on computer vision and pattern recognition. pp. 1125–1134 (2017)
11. Johnson, J., Alahi, A., Fei-Fei, L.: Perceptual losses for real-time style transfer and super-resolution. In: European conference on computer vision. pp. 694–711. Springer (2016)
12. Khan, A.M., Rajpoot, N., Treanor, D., Magee, D.: A nonlinear mapping approach to stain normalization in digital histopathology images using image-specific color deconvolution. *IEEE Transactions on Biomedical Engineering* **61**(6), 1729–1738 (2014)
13. Khan, A.M., Rajpoot, N., Treanor, D., Magee, D.: A nonlinear mapping approach to stain normalization in digital histopathology images using image-specific color deconvolution. *IEEE Transactions on Biomedical Engineering* **61**(6), 1729–1738 (2014)
14. Larsen, A.B.L., Sønderby, S.K., Larochelle, H., Winther, O.: Autoencoding beyond pixels using a learned similarity metric. arXiv preprint arXiv:1512.09300 (2015)
15. Macenko, M., Niethammer, M., Marron, J.S., Borland, D., Woosley, J.T., Guan, X., Schmitt, C., Thomas, N.E.: A method for normalizing histology slides for quantitative analysis. In: 2009 IEEE International Symposium on Biomedical Imaging: From Nano to Macro. pp. 1107–1110. IEEE (2009)
16. Macenko, M., Niethammer, M., Marron, J.S., Borland, D., Woosley, J.T., Guan, X., Schmitt, C., Thomas, N.E.: A method for normalizing histology slides for quantitative analysis. In: 2009 IEEE International Symposium on Biomedical Imaging: From Nano to Macro. pp. 1107–1110. IEEE (2009)
17. Magee, D., Treanor, D., Crellin, D., Shires, M., Smith, K., Mohee, K., Quirke, P.: Colour normalisation in digital histopathology images. In: Proc Optical Tissue Image analysis in Microscopy, Histopathology and Endoscopy (MICCAI Workshop). vol. 100, pp. 100–111. Citeseer (2009)
18. Mao, X., Li, Q., Xie, H., Lau, R.Y., Wang, Z., Paul Smolley, S.: Least squares generative adversarial networks. In: Proceedings of the IEEE International Conference on Computer Vision. pp. 2794–2802 (2017)
19. Niethammer, M., Borland, D., Marron, J., Woosley, J., Thomas, N.E.: Appearance normalization of histology slides. In: International Workshop on Machine Learning in Medical Imaging. pp. 58–66. Springer (2010)
20. Reinhard, E., Adhikhmin, M., Gooch, B., Shirley, P.: Color transfer between images. *IEEE Computer graphics and applications* **21**(5), 34–41 (2001)
21. Ronneberger, O., Fischer, P., Brox, T.: U-net: Convolutional networks for biomedical image segmentation. In: International Conference on Medical image computing and computer-assisted intervention. pp. 234–241. Springer (2015)
22. Shaban, M.T., Baur, C., Navab, N., Albarqouni, S.: Staingan: Stain style transfer for digital histological images. arXiv preprint arXiv:1804.01601 (2018)
23. Xiao, X., Lian, S., Luo, Z., Li, S.: Weighted res-unet for high-quality retina vessel segmentation. In: 2018 9th International Conference on Information Technology in Medicine and Education (ITME). pp. 327–331. IEEE (2018)

24. Zhu, J.Y., Park, T., Isola, P., Efros, A.A.: Unpaired image-to-image translation using cycle-consistent adversarial networks. In: Proceedings of the IEEE international conference on computer vision. pp. 2223–2232 (2017)